Knowledge Empowerment Foundation
Empowering Knowledge
www.kemfo.org

EXPLORATORY MATERIALS SCIENCE RESEARCH

E-ISSN : 2582-8444

Original Research Article

EMSR, 1(1) 2020 [57-66]

Nanorod hierarchical structures of 3D flower-like ZnO nanoparticles and their structurally-influenced superhydrophobicities

Tayirjan T.Isimjan[1,2,4], Quan Ge[1], Edward Sacher[3], De-Quan Yang[1]*

[1]Solmont Technology Wuxi Co., Ltd. 228 Linghu Blvd., Tianan Tech Park, A1-602, Xinwu District, Wuxi, Jiangsu 214135, (CHINA)

[2]Division of Physical Sciences and Engineering, Solar and Photovoltaics Engineering Center, King Abdullah University of Science and Technology (KAUST), Thuwal 23955-6900, (SAUDI ARABIA)

[3]Regroupement Québécois de Matériaux de Pointe, Départementde Génie Physique, Polytechnique Montréal, Case Postale 6079, Succursale Centre-Ville, Montréal, Québec H3C 3A7, (CANADA)

[4]Present address: SABIC-Corporate Research and Development Center (CRD) at KAUST, Thuwal 23955, (SAUDI ARABIA)

E-mail: dequan.yang@gmail.com

DOI : https://dx.doi.org/10.47204/EMSR.1.1.2020.057-066

ABSTRACT

A simple aqueous solution process, employing triethylene glycol (TEG) and sodium hydroxide (NaOH), was used to synthesize zinc oxide (ZnO) powder, whose 3D flower-like structure self-assembled into larger scale nanorod hierarchical nanostructures. The influences of various reaction parameters on the crystal structures and morphologies of the resulting products were investigated. The samples were characterized by X-ray diffraction (XRD), field emission scanning electron microscopy (FESEM), and high-resolution transmission electron microscopy (HRTEM). We found that the hierarchical ZnO nano/microstructures could be precisely controlled by adjusting the experimental parameters. Further, coatings prepared from two typical hierarchical ZnO flower-like structures showed high levels of superhydrophobicity on treatment with stearic acid. Superhydrophobicity values differed for different morphologies, attributed to the synergistic effects of the ratios of the dual structures formed. This leads to a simple, scalable, low-temperature aqueous solution synthesis route for flower-like zinc oxide, which is then self-assembled into nanorod blocks, intended for superhydrophobic coating applications.

KEYWORDS

Flower-like; Nanostructures; Superhydrophobic surfaces; ZnO.

INTRODUCTION

The shape, crystalline structure and size of a nanomaterial all play an important role in determining its physical and chemical properties[1,2], and the rational control of these features has become an important topic of research[3-5]. Nanostructured ZnO materials, including nanoparticles, have potential industrial applications in self-cleaning coatings[6-9], solar cells[10-12], sensors[13-15], ceramics[16], biology and medicine[17-19], and other fields. It is a recognized fact that the two essential factors for achieving superhydrophobic surfaces are surface

roughness and low surface energy coatings. Particularly in the case of superhydrophobic coatings, nanostructured ZnO has some unique properties, such as antifungal activity and ultraviolet radiation degradation resistance. Although one such ZnO nanostructure, with raspberry-like morphology, is already used for constructing superhydrophobic surfaces[20,21], it is difficult to produce such nanostructures using conventional methods.

It has been demonstrated that ZnO with nano-/microstructural crystal morphologies such as wires, rods, needles, columns, tubes, springs, belts, tetrapod, etc., can be fabricated, mostly by gas-phase reactions[22-29]. Flower-like, dual-sized hierarchical ZnO structures[30-32] constitute the ideal morphology for superhydrophobic coating because of their high surface area, good dispersibility and an excellent embedding ability in coating materials. However, most such fabrications require either high temperatures or extended reaction times, making them unsuitable for industrial applications. To overcome this, it is necessary to develop a simple, low-cost, scalable fabrication process.

Low temperature, aqueous solution routes have shown great promise for the synthesis of inorganic materials[33-36]. Such methods may constitute the simplest and most effective ways to scale up well-crystallized ZnO nano-/microstructured materials with specific morphologies, at a relatively low temperature.

Herein, we describe a simple, scalable, low-temperature aqueous solution route for the synthesis of flower-like ZnO, self-assembled by nanorod blocks, for intended application in superhydrophobic coatings, in contrast to methods commonly reported in the literature[22-29]. Our results reveal that rod-like and flower-like ZnO may be fabricated by fine-tuning the experimental parameters, followed by surface modification.

MATERIALS AND METHODS

Preparation of nanostructured ZnO

The reagents were analytical grade, used as purchased. Deionized (DI) water, produced by ion exchange, with a resistance > 18 M&Ω, was used to make a 1M aqueous zinc acetate ($Zn(CH3CO_2)_2$) solution. In a typical process, 2.26g of NaOH were dissolved in 50 mL of deionized water, and 4 mL of 1M $Zn(CH3CO_2)_2$ were added at room temperature, with magnetic stirring. A white precipitate immediately appeared but dissolved on further stirring. Ten mL of triethylene glycol (TEG) were added to the solution, and stirred for 2 min. The mixed solution was then permitted to stand at room temperature, during which time a precipitate formed. The precipitate was collected by centrifugation, washed at least five times with DI water and ethanol, and dried at 60°C for 10 h. To investigate the effects of preparation conditions on the samples, several experimental parameters, such as the amounts of NaOH and TEG added, the volumetric ratio of TEG to DI water, the reaction temperature and precipitation time, were varied.

The preparation of superhydrophobic ZnO thin films

To investigate the superhydrophobicity of the ZnO precipitate, the surfaces of the as-prepared materials were functionalized with stearic acid. In a typical procedure, 2 g of ZnO powder and 0.3680 g of stearic acid were dispersed in 20 mL of ethanol, with constant stirring for 30 min at room temperature, and then aged for 1-2 h. The suspension was then used to fabricate thin films by dip coating glass slides, which was dried in an oven, at 75°C, to form a uniform, flat thin film. To understand the effect of different sizes and morphologies of ZnO, and the role of stearic acid, a series of films, with different stearic acid contents, was prepared.

Characterization

The crystal structures of the synthesized products were examined by X-ray diffraction (XRD), using a Bruker D8 Advance X-ray diffractometer. The XRD patterns were recorded in the 2θ range 20-80°, with a scanning step of 0.03°. The morphologies and sizes of the products were characterized with a JEOL JSM-5900 field-emission scanning electron microscope (FESEM), using an acceleration voltage of 10 kV. The detailed microstructures of the products were examined by a JEOL 4000EX high resolution transmission electron microscopy (HRTEM), operated at 400 keV. These samples were tested for superhydrophobicity, using a Shanghai Suolun Scientific Instruments SL200B contact angle goniometer. Each of the reported values for water contact angle (CA) and sliding angle (SA)

was obtained by averaging five measurement results, using 5 μL droplets, on different areas of the samples.

RESULTS AND DISCUSSION

Morphologies and structures of ZnO powders

Typical SEM and TEM photomicrographs of a ZnO powder are found in Figure 1. The morphology of the ZnO is flower-like, self-assembled from nanorod building blocks. The flowers are relatively uniform, with diameters of 2-3 μm. The diameters of the nanorods are several hundred nm, with sharp ends. The TEM photomicrograph shows the single crystal structure of these rods, indicating rod growth along the [2000] direction.

Influence of the preparation conditions on morphology

The structure of the ZnO powder is very sensitive to each of the experimental conditions. We performed detailed studies on the effect of each parameter, keeping the others constant.

Effect of sodium hydroxide (NaOH)

The results on varying the amount of NaOH used are found in TABLE 1.

The sample morphologies were characterized by FESEM. The photomicrographs (see Figure S2) show a flower-like structural assembly of nanorods, with all the samples showing a significant hierarchical nano-dendritic structure. However, the aspect ratio of the nanorods increased with increasing NaOH concentration, and the flower-like nanostructures began to disassemble above a NaOH concentration of 0.045 g/ml, where the nanoparticles appeared to be composed of loose nanorods. That is, higher NaOH concentrations resulted in the loss of self-assembly, apparently by ZnO dissolution; similar results were reported by Yogamalar

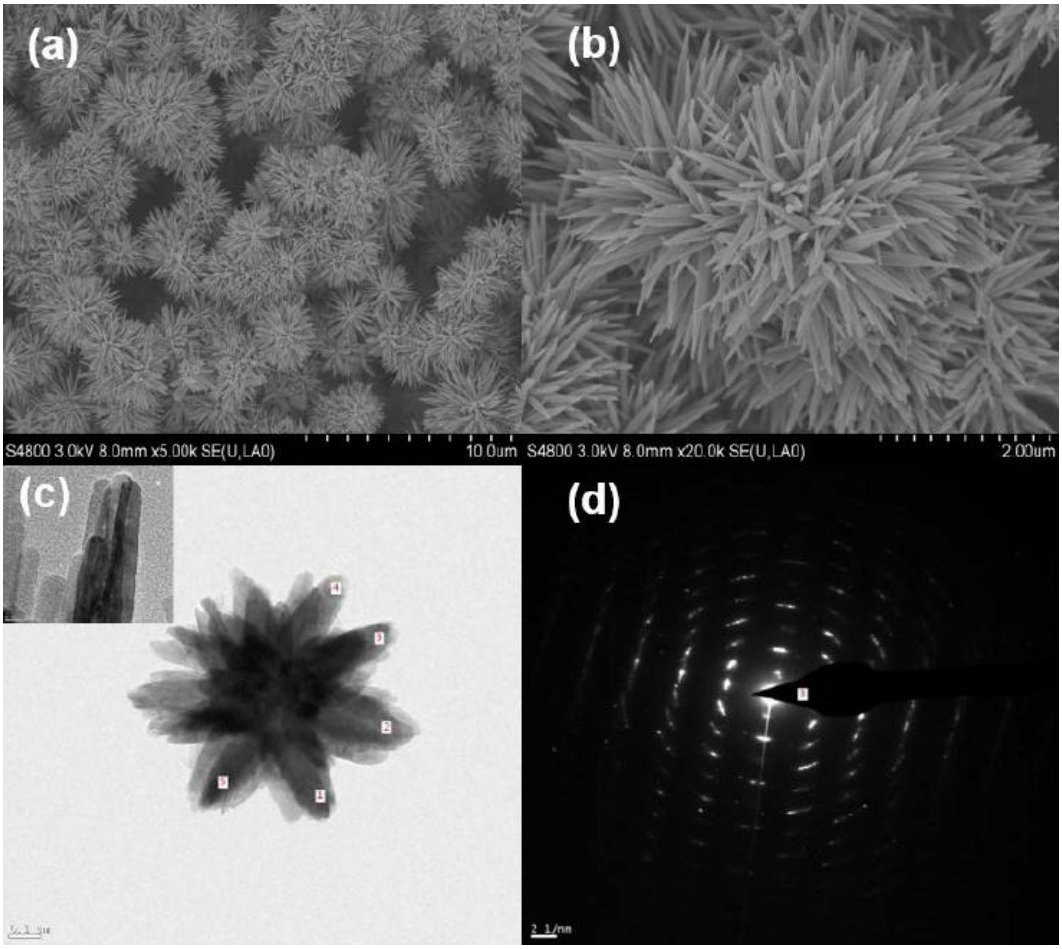

Figure 1: SEM images of a typical flower-like ZnO powder: (a) 5000 X (b) 20000X. TEM images: (c) flower-like morphology and (d) selected area electron diffraction (SAED) pattern.

et al.[37] using a hydrothermal process. In addition, Hou et al.[38] reported a similar phenomenon when they prepared flower-like ZnO microspheres by a low-temperature alkaline solution route, using PEG. Consequently, the NaOH concentration was kept constant, at 0.038 g/mL, during the rest of the experiments.

Effect of reaction temperature

TABLE 2 summarizes the effect of temperature on the ZnO microstructure. As the reaction temperature increased, the flower-like morphology changed from nanoflakes to nanorods.

SEM photomicrographs of the effect of the reaction temperature, ranging from 10 to 80ºC, on the ZnO morphology are shown in Figure 3. At 10ºC, nanoflakes, having a uniform thickness of about 50 nm, overlap and self-assemble into a discernible ball-of-yarn morphology (Figure 3a); these nanoflakes show excellent superhydrophobicity, as reported elsewhere[39]. Flower-like nanostructures appear at 50ºC. as seen in Figures 3c and 4d. Their dimensions are approximately 4 μm, and the nanorods display an irregular morphology. The aspect ratio of the nanorods is greater than those fabricated at 30ºC. In addition, as expected, the ZnO

TABLE 1: The effect of the amount of NaOH on the ZnO morphology

Samples	NaOH[a]		ZnO Morphologies[b]
	g	g/mL (solution)	
1-1	1.12	0.022	Flower-like structure, composed of low aspect ratio nanorods with sharp tips
1-2	1.7	0.034	Flower-like structure, composed of higher aspect ratio nanorods with sharp tips
1-3	2.26	0.045	Flower-like structure composed of higher aspect ratio nanorods with sharp tips
1-4	3.4	0.068	A mixture of flower-like and nanorod structures, having the highest aspect ratio nanorods with sharp tips.

[a] The amount of sodium hydroxide; [b] Observed by FESEM; 1M $Zn(CH_3CO_2)_2$ solution and TEG were fixed at 50mL and 10 mL, respectively, and the reaction time and reaction temperature were 24 h and 30°C, respectively.

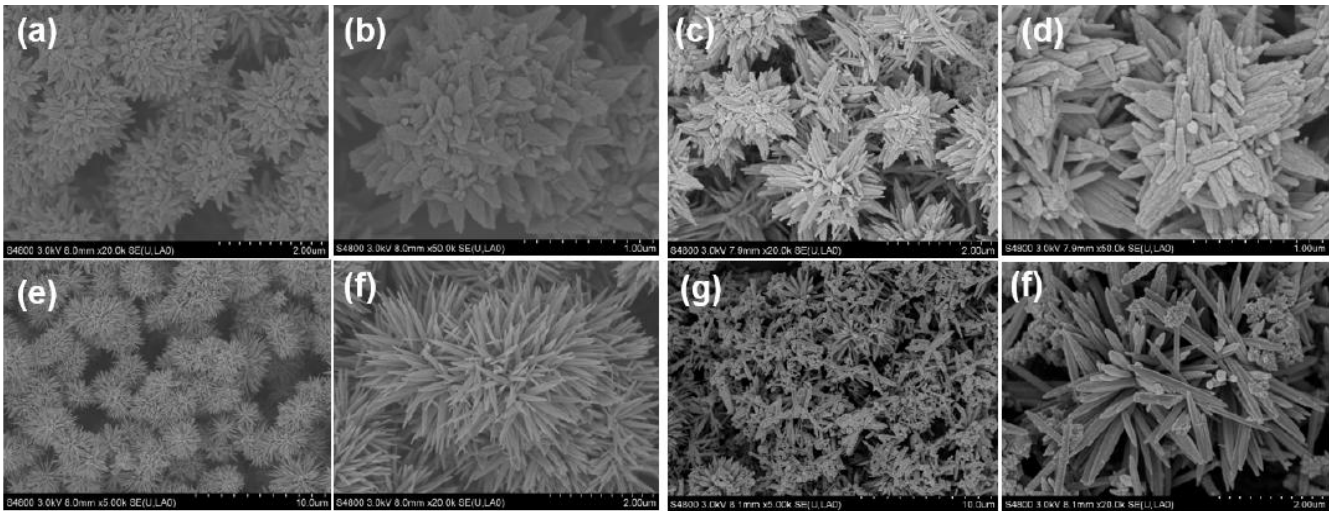

Figure 2: FESEM micrographs of the samples prepared with various NaOH contents. (a) and (b) Sample 1-1, (c) and (d) Sample 1-2, (e) and (f) Sample 1-3, (g) and (h) Sample 1-4, all at several magnifications.

TABLE 2: The effect of the reaction temperature on ZnO product morphology and duration.

Samples	Temperature (°C)	Time (h)	ZnO Morphologies[a]
2-1	10	24	Flower-like structure, composed of low aspect ratio nanorods
2-2	50	6	Flower-like structure, composed of higher aspect ratio nanorods with sharp tips
2-3	80	2	Flower-like structure, composed of highest aspect ratio nanorods with sharp tips

[a] NaOH was fixed at 2.26 g (0.038 g/mL); TEG and 1M $Zn(CH_3CO_2)_2$ solutions were fixed at 10 mL and 50 mL, respectively. Morphologies are based on Figure 4.

formation reaction time became shorter with increased temperature, as the reaction rate increased. Figures 3e and 3f further confirm that the temperature has a significant influence on the morphology (Figure 3, Sample 2-3). With the increase in temperature, the nanorods lost their ability to self-assemble. Rod lengths of 6-10 μm, and diameters of 0.7-1.1 μm were obtained when the temperature was increased to 80ºC, at which the total synthesis time was only 2 h. These results show that a suitable reaction temperature is a critical factor to control both reaction rate and morphology. Increasing the reaction temperature not only facilitated the conversion of nanoparticles to nanorods, but also inhibited the ability of self-assembly into a desired morphology. There is a trade-off between shortening the reaction time and keeping the hierarchical morphology that results in the best superhydrophobicity.

Effect of TEG

TEG is a directional growth reagent that plays an important role in the morphology of the nanoparticles, as shown in the SEM photomicrographs in Figure 4, for samples prepared at various TEG volume ratios (TABLE 3). Because there was no ZnO formation without TEG at 30ºC, the temperature was increase to 80°C. Flower-like nanoparticles, 2–3 μm, composed of loose and disordered nanorods, were formed after 4 hours.

Regular hexagonally shaped nanorods were formed on the addition of 5 mL of TEG (Figure 4c and d). The resulting nanoparticles have sizes similar to those in Figure 3f. They tended to bunch when the TEG volume was increased to 20 mL Sample 3-), shown in Figures 4e

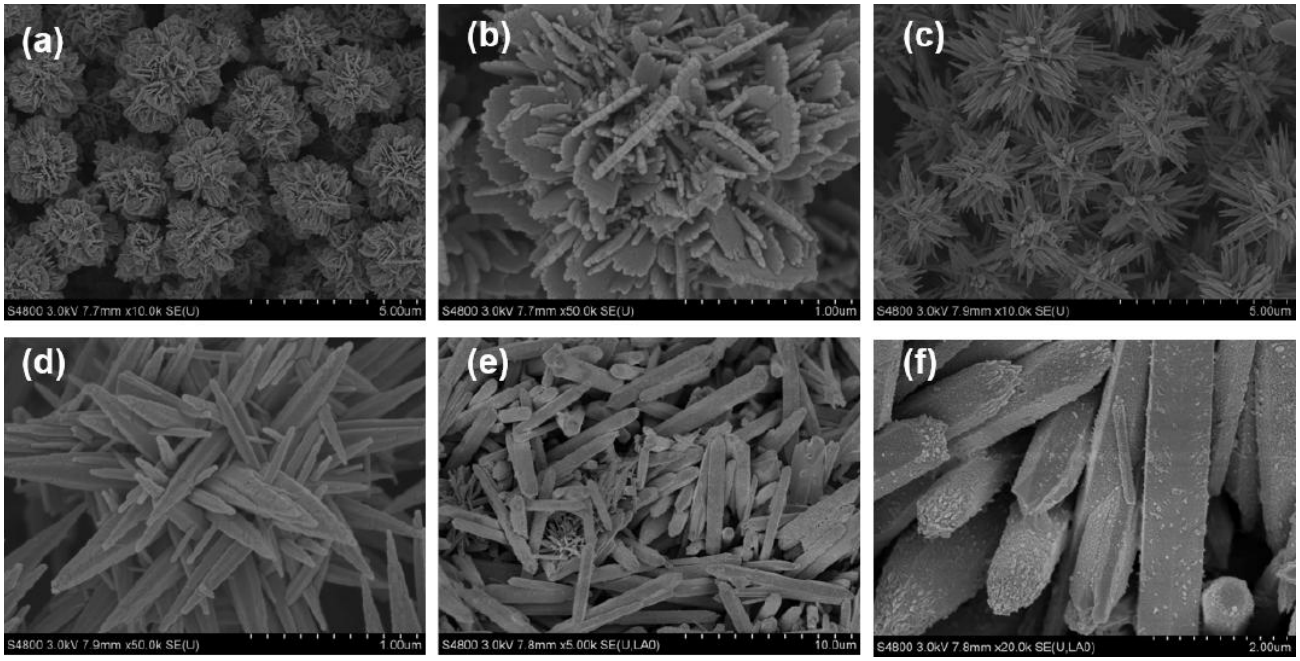

Figure 3: FESEM micrographs of samples at different reaction temperatures (10-80°C) and durations (2-24h): (a) and (b) Sample 2-1, (c) and (d) Sample 2-2, (e) and (f) Sample 2-3, all at several magnifications.

TABLE 3: The effect of the amount of TEG on sample morphology.

Samples[a]	TEG		ZnO Morphologies
	mL	mL/mL(H_2O)	
3-1	0	0	Small flower-like structures, assembled from low aspect ratio (2.5:1) nanorods with sharp tips
3-2	5	0.1	Large flower-like structures, assembled from higher aspect ratio (6:1) nanorods with sharp tips
3-3	20	0.4	Large flower-like structures, assembled from higher aspect ratio (7:1) nanorods with sharp tips
3-4	30	0.6	Large flower-like structures, assembled from higher aspect ratio (6:1) nanorods with sharp tips

[a] NaOH was fixed at 0.038 g/mL; 1M $Zn(CH_3CO_2)_2$ solution was kept at 50 mL, reaction temperature was 30°C (except for sample S3-1, which was 8 0°C because no ZnO formed at 30°C). Reaction time was 24 h (except for sample S2-1, which was 2 h). The highest TEG/water ratio was 0.6:1.

and f, and dendritic nanostructures, with sizes of 3–5 μm, were obtained. Figure 4e shows the powders to be composed of dense nanorods, as in Figure 3b, with many smaller nanorods grouped to form a single bundle. A further increase in the TEG volume resulted in the loss of nanorod self-assembly and a reduced formation of flower-like structures. These results indicate that a higher reaction temperature and a higher volume ratio of TEG led to rapid crystal growth, giving longer, larger nanorods.

Effects of high concentrations of TEG and NaOH at high temperatures

To synthesize high quality flower-like structures with high aspect ratio nanorods, in a short period, the TEG/H_2O ratio was increased substantially at 80°C, as was the NaOH/H_2O ratio.

The SEM photomicrographs of Figure 5 reveal that the 80ºC reaction temperature appeared to be optimum to synthesize flower-like nanostructures rapidly at high concentrations of both TEG and NaOH. To maintain the stability of the precursor solution during heating, we reduced the amount of water to 10 mL, and the TEG was preheated to 80ºC before mixing. The effect of the TEG/1M $Zn(CH_3CO_2)_2$ solution ratio on the sample morphology is shown in TABLE 4, indicating that the most suitable condition for rapidly synthesizing flower-like ZnO nanoparticles, in large quantities, was T (80°C), TEG (67 v/v %), and NaOH (0.26 g/mL) in 1M $Zn(CH_3CO_2)_2$ solution.

The FESEM photomicrographs in Figure 5 may be compared with the sample XRD patterns Figure 6. As seen in Figure 5, when the TEG/water ratio was 3:1, the product was mostly composed of 50-100 nm nanoparticles, along with a small amount of nanorods with lengths of tens of nanometers (Figures 5a, Sample 4-1), without any tendency to self-assemble. A TEG/water ratio of 2.5:1 produced a large number of nanoparticles, along with some flower-like nanostructures composed of bundled nanorods (Figures 5b, Sample 4-2). When the TEG/water ratio was 2:1, regular nanorods and flower-like ZnO nanostructures,

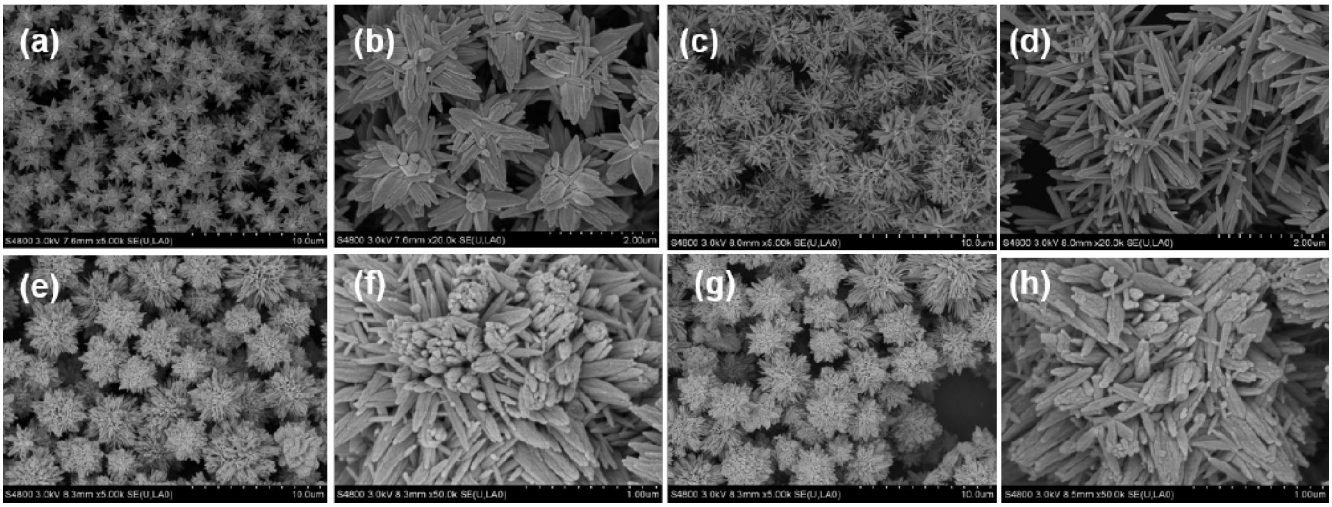

Figure 4: FESEM micrographs of the as-prepared samples with various TEG contents: (a) and (b) Sample 3-1, (c) and (d) Sample 3-2, (e) and (f) Sample 3-3, (g) and (h) Sample 3-4, all at several magnifications.

TABLE 4: A summary of the effects of the ratios of reaction medium on the ZnO morphologies

Samples	TEG/H_2O[a]	ZnO morphologies
4-1	3:1	50-100 nm nanoparticles.
4-2	2.5:1	Aggregated nanoparticles, early stage of flower-like structures.
4-3	2:1	Flower-like powder, self-assembled from low aspect nanorods with sharp tips
4-4	1.5:1	Both flower-like powder and nanorods, the flowers containing low aspect ratio nanorods, with some loss of self-assembly.
4-5	1:1	Nanorods, with complete loss of self-assembly.

[a] **Triethylene glycol/deionized water volumetric ratio; NaOH/1M $Zn(CH_3CO_2)_2$ solution ratio was fixed at 0.23 g/mL, water was kept at 10 mL, and reaction temperature and time were kept at 80°C and 2 h, respectively.**

700 nm in diameter, were observed, as exemplified by Sample 4-3 in Figures 5c and d. The diameters of the nanorods were 50-200 nm, with lengths of 100-400 nm. When the ratio was further decreased to 1.5:1 and 1:1, respectively, there was no flower-like material formed, but only loose nanorods, indicating that higher ratios resulted in a loss of self-assembly. Figure 5f shows large nanorods, with a width of 100 nm and a length of up to 1 μm. These observations indicate that the TEG/water ratio plays a key role in the formation of the various structures. In addition, the NaOH concentration appears to influence the lengths of the nanorods. As shown in Figure 5 and TABLE 4, the TEG acts as an attracting agent during ZnO formation, and higher TEG concentrations resulted in an increased density of ZnO nanoparticles. Undesirable nanorods also formed when the TEG concentration was too high, as shown in Figures 5g-h. However, a low TEG concentration led to a low density of ZnO nuclei, and retarded nanorod growth and self-assembly, as seen in Figure 5f. The condition that produced a high density of ZnO nuclei, and resulted in a mainly flower-like morphology product, is seen in Figure 5e-f. Accordingly, the optimization of the dimensions of the flower-like powder, self-assembled from the nanorods, as well as the nanorod aspect ratios, were all controlled by the TEG concentration.

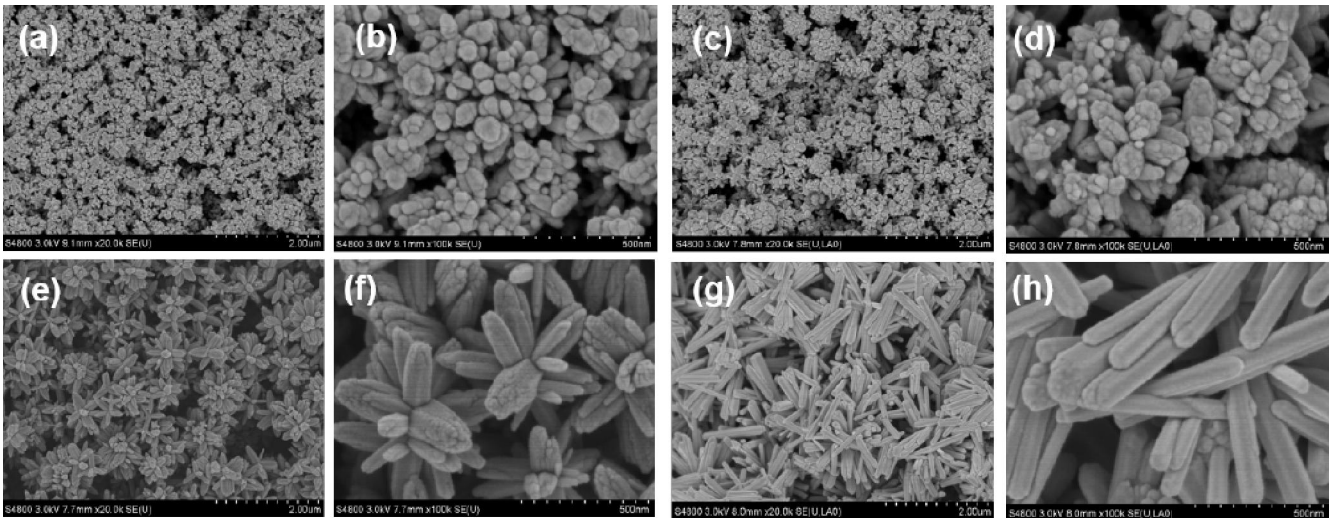

Figure 5: FESEM micrographs of as-prepared ZnO at two different magnifications in various TEG/W volumetric ratios: (a) Sample 4-1, (b) Sample 4-2, (c) and (d) Sample 4-3, (e) and (f) Sample 4-4, (g) and (h) Sample 4-5.

XRD analysis

As shown in Figure 6, each XRD pattern can be indexed to the pure wurtzite structure of ZnO, with lattice constants of a = 3.249 Å and c = 5.206 Å, consistent with the values on the standard card (JCPDS No. 36-1451). No impurity peaks were observed. Furthermore, the diffraction peaks are intense and narrow, indicating that the ZnO has a high level of crystallinity and a large crystal size. The greater the TEG/solution volume ratio, the greater the intensity ratio of the peak at 34.4º (002) to that at 35.3º (001), due to crystal growth along the [0001] direction. For instance, the peak intensity ratio of (002)/(001) increased from 0.54 to 0.75 when the TEG/solution volume ratio changed from 1:1 to 3:1, indicating nanorod formation[40].

The crystal sizes, in nm, were determined using the

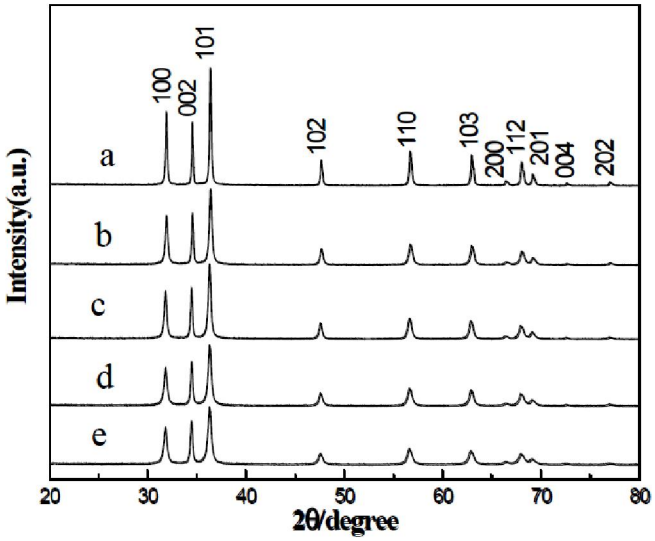

Figure 6: X-ray diffraction patterns of the as-prepared samples at different TEG/water ratios at 80°C. (a) 3:1, (b) 2.5:1, (c) 2:1, (d) 1.5:1, and (e) 1:1.

Original Research Article

Debye-Scherrer equation, Eqn. (1)[41]:

$$D = \frac{K\lambda}{\beta.Cos\theta} \quad (1)$$

where D is the crystalline size (nm), *K* is the shape factor (taken as 0.9), λ is the wavelength of Cu Kα radiation (0.154056 nm), *β* is the instrumental broadening, which is taken as the full width at half maximum (fwhm) of the corresponding peak in radians, and θ is the Bragg diffraction angle. The strain induced in the crystal lattice, caused by crystal imperfection and distortion, was calculated using the Williamson-Hall equation, Eqn. (2)[42]:

$$\varepsilon = \frac{\beta}{4tan\theta} \quad (2)$$

Both the crystal sizes and the strains of the samples in TABLE 4 are shown in Figure 7. The results show that the ZnO crystallite size increased with increasing TEG concentration, although the lattice strain increased as the crystallite size decreased, because the smaller crystal size has a higher surface energy. Interestingly, both the crystallite size and the lattice stain follow linear trends with increasing TEG, until a TEG ratio of 75%, indicating the point at which one crystal growth regime changes to another; that is, where the morphology changes from nanorods caused by C-axis directional growth, to spherical, resulting from multidirectional crystal growth, as verified in Figure 5

Previous results exist on the superhydrophobic properties of nanostructured ZnO surfaces[43,44], using different surface treatments. For comparison, we selected Samples 1-3 (Figure 2) and 4-3 (Figure 5); both have flower-like morphologies of different sizes, and nanorods of different aspect ratios. Their surfaces were treated with stearic acid[39]. Figure 8 shows the water contact (CA) and sliding (SA) angles of the samples with different quantities of stearic acid[45]. While all samples show superhydrophobic properties, the CAs increased with increasing stearic acid content. When the molar ratio of stearic acid to ZnO increased to 6%, the water CA of Sample 1-3 reached a maximum value of ~ 160°, with a low SA of ~ 2° (Figure 7a), and when the molar ratio of stearic acid to ZnO increased to 10%, the water CA of Sample 4-3 reached a maximum value of ~ 157°, with a very low SA of ~ 1°.

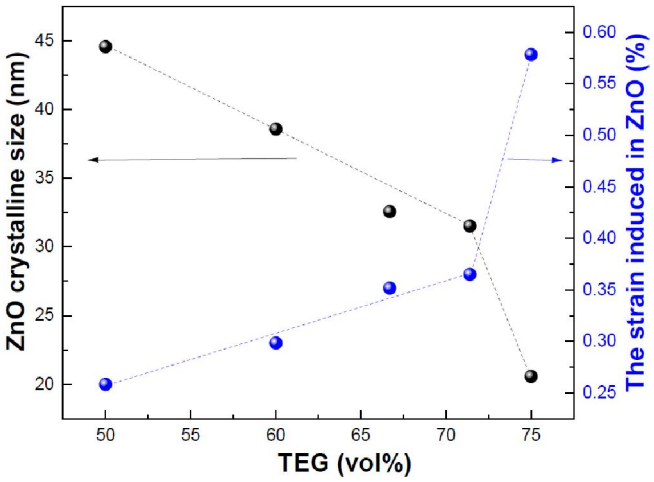

Figure 7: Trends in crystallite size and lattice stain, as a function of the TEG ratio.

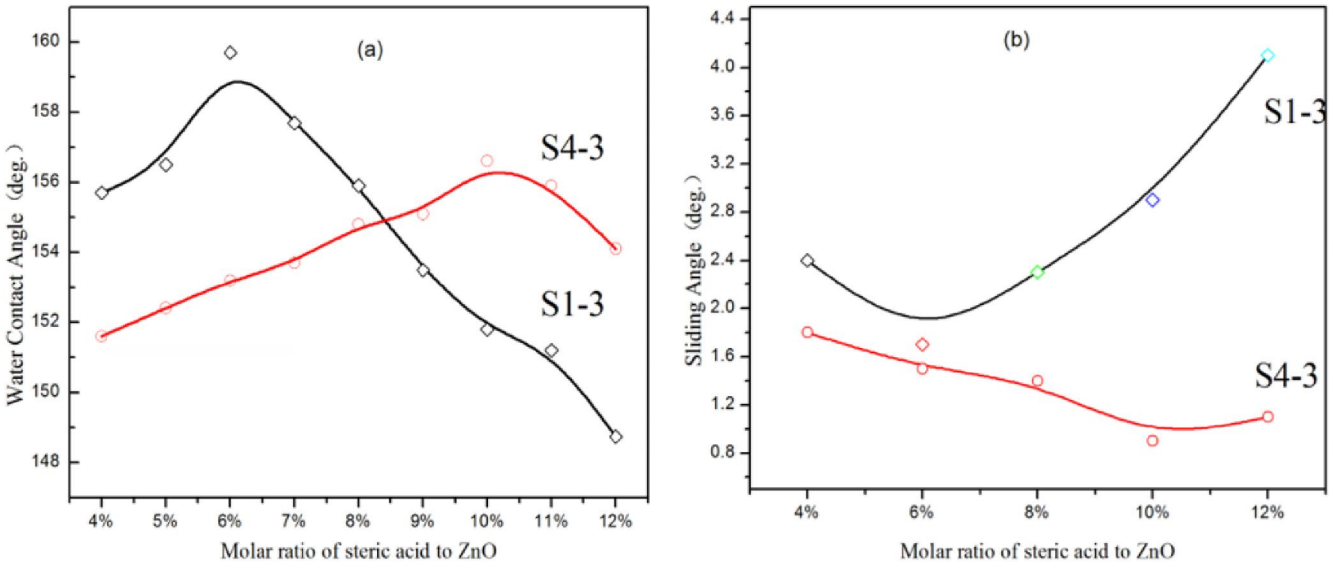

Figure 8: Sample CAs (a), and SAs (b) as a function of stearic acid content.

However, the water CA decreased as the stearic acid content was further increased.

Figure 8b shows the water SA values of the as-prepared superhydrophobic surface; the SA values of 700 nm size of flower-like ZnO (Figure 5, Sample 4-3) were determined to be ~ 1-2°, which is markedly lower than those (~ 2-4°) of Samples 1-3 (Figure 2). This difference appears to be due to their nanoscale structural dissimilarities: although the samples have similar rod-like and flower-like morphologies, their nanorod sizes and densities are different. The high level of superhydrophobicity (larger CA and smaller SA) of the hierarchic ZnO nanostructures reveals their potential application to superhydrophobic coatings. More importantly, different particle sizes showed their respective advantages, which may be extended to other nanomaterials, for use in superhydrophobic coatings.

CONCLUSIONS

We have developed a facile and economic route to the scalable synthesis of rod-like and flower-like ZnO nanostructures, through the fine-tuning of the various reaction parameters. For practical applications, such as the production of superhydrophobic materials, the appropriate reactant concentrations and reaction temperature are key synthesis parameters. Superhydrophobicity was produced by treatment with stearic acid, with the best values being a static water contact angle of 160° and a sliding angle of 2°.

ACKNOWLEDGEMENTS

The authors express their appreciation to Wuxi City Technology Innovation Foundation, TTI is grateful for support from KAUST for this work.

REFERENCES

[1] T.Li, J.Wang, Y.Zhang; J.Nanosci.Nanotechnol., **5**, 1435-1447 **(2005)**.
[2] Z.Xu, L.Wang, F.Fang, Y.Fu, Z.Yin; Current Nanosci., **12**, 725-746 **(2016)**.
[3] L.Q.Cheng, J.F.Li; J.Materiomics, **2**, 25-36 **(2016)**.
[4] L.Li, L.Liang, H.Wu, X.Zhu; Nanoscale Res.Lett., **11**, 1-17 **(2016)**.
[5] I.Udom, M.K.Ram, E.K.Stefanakos, A.F.Hepp, D.Y.Goswami; Materials Science in Semicond. Proc., **16**, 2070-2083 **(2013)**.
[6] X.Gao, Z.Guo; J.Bionic Eng., **14**, 401-439 **(2017)**.
[7] C.Mondal, M.Ganguly, A.K.Sinha, J.Pal, T.Pal; RSC Advances, **3**, 5937-5944 **(2013)**.
[8] Y.Xin, Z.Guo; Chem.Lett., **43**, 305-306 **(2014)**.
[9] Y.Gao, I.Gereige, A.El Labban, D.Cha, T.T.Isimjan, P.M.Beaujuge; ACS Appl.Mater. Interfaces, **6**, 2219-2223 **(2014)**.
[10] K.Kaur, N.Kumar, M.Kumar; J.Mater.Chem.A, **5**, 3069-3090 **(2017)**.
[11] X.Liu, J.Iocozzia, Y.Wang, X.Cui, Y.Chen, S.Zhao, Z.Li, Z.Lin; Energy Environ.Sci., **10**, 402-434 **(2017)**.
[12] R.Vittal, K.C.Ho; Renew.Sustain.Energy Rev., **70**, 920-935 **(2017)**.
[13] A.Bertuna, G.Faglia, M.Ferroni, N.Kaur, H.M.M.M.Arachchige, G.Sberveglieri; E.Comini, Sensors (Switzerland), **17**, 1000 **(2017)**.
[14] G.Gasparotto, J.P.C.Costa, P.I.Costa, M.A.Zaghete, T.Mazon; Mater.Sci.Eng.C, **76**, 1240-1247 **(2017)**.
[15] M.Laurenti, S.Stassi, G.Canavese, V.Cauda; Adv. Mater.Interfaces, **4**, 1600758 **(2017)**.
[16] S.Y.Sokovnin, V.G.Il'ves, V.R.Khrustov, M.G.Zuev; Ceram.Internat., **43**, 10637-10644 **(2017)**.
[17] L.Cheng, K.Zhang, M.D.Weir, M.A.S.Melo, X.Zhou, H.H.K.Xu; Nanomed., **10**, 627-641 **(2015)**.
[18] E.Hoseinzadeh, P.Makhdoumi, P.Taha, H.Hossini, J.Stelling, M.A.Kamal, G.M.Ashraf; Curr.Drug Metab., **18**, 120-128 **(2017)**.
[19] S.R.Saptarshi, A.Duschl, A.L.Lopata; Nanomed., **10**, 2075-2092 **(2015)**.
[20] W.Ming, D.Wu, R.Van Benthem, G.De With; Nano Lett., **5**, 2298-2301 **(2005)**.
[21] Z.Qian, Z.Zhang, L.Song, H.Liu; J.Mater.Chem., **19**, 1297-1304 **(2009)**.
[22] Y.H.Chou, B.T.Chou, C.K.Chiang, Y.Y.Lai, C.T.Yang, H.Li, T.R.Lin, C.C.Lin, H.C.Kuo, S.C.Wang, T.C.Lu; ACS Nano, **9**, 3978-3983 **(2015)**.
[23] M.H.Huang, S.Mao, H.Feick, H.Yan, Y.Wu, H.Kind, E.Weber, R.Russo, P.Yang; Science, **292**, 1897-1899 **(2001)**.
[24] P.Yang, H.Yan, S.Mao, R.Russo, J.Johnson, R.Saykally, N.Morris, J.Pham, R.He, H.J.Choi; Adv.Funct.Mater., **12**, 323-331 **(2002)**.
[25] L.Guo, Y.L.Ji, H.Xu, P.Simon, Z.Wu; J.Amer. Chem.Soc., **124**, 14864-14865 **(2002)**.

Original Research Article

[26] W.I.Park, G.C.Yi, M.Kim, S.J.Pennycook; Adv. Mater., **14**, 1841-1843 **(2002)**.
[27] Z.R.Tian, J.A.Voigt, J.Liu, B.McKenzie, M.J.McDermott; J.Amer.Chem.Soc., **124**, 12954-12955 **(2002)**.
[28] P.X.Gao, Z.L.Wang; Small, **1**, 945-949 **(2005)**.
[29] P.Zheng Wei, D.Zu Rong, W.Zhong Lin; Science, **291**, 1947-1949 **(2001)**.
[30] R.C.Pawar, J.S.Shaikh, A.A.Babar, P.M.Dhere, P.S.Patil; Solar Ener., **85**, 1119-1127 **(2011)**.
[31] S.Chakraborty, A.K.Kole, P.Kumbhakar; Mater. Lett., **67**, 362-364 **(2012)**.
[32] D.E.Motaung, G.H.Mhlongo, S.S.Nkosi, G.F.Malgas, B.W.Mwakikunga, E.Coetsee, H.C.Swart, H.M.I.Abdallah, T.Moyo, S.S.Ray; ACS Appl.Mater.Interfaces, **6**, 8981-8995 **(2014)**.
[33] S.T.Meyers, J.T.Anderson, C.M.Hung, J.Thompson, J.F.Wager, D.A.Keszler; J.Amer. Chem.Soc., **130**, 17603-17609 **(2008)**.
[34] L.P.Bauermann, J.Bill, F.Aldinger; J.Phys.Chem.B, **110**, 5182-5185 **(2006)**.
[35] J.J.Richardson, F.F.Lange; J.Mater.Chem., **21**, 1859-1865 **(2011)**.
[36] C.B.Tay, J.Tang, X.S.Nguyen, X.H.Huang, J.W.Chai, V.T.Venkatesan, S.J.Chua; J.Phys. Chem.C, **116**, 24239-24247 **(2012)**.
[37] N.Rajeswari Yogamalar, A.Chandra Bose; J.Solid State Chem., **184**, 12-20 **(2011)**.
[38] X.Hou, F.Zhou, B.Yu, W.Liu; Mater.Lett., **61**, 2551-2555 **(2007)**.
[39] Y.Wang, B.Li, C.Xu; Superlatt.Microstruct., **51**, 128-134 **(2012)**.
[40] Y.Feng, M.Zhang, M.Guo, X.Wang; Cryst.Growth Des., **10**, 1500-1507 **(2010)**.
[41] Y.R.Guo, F.D.Yu, G.Z.Fang, Q.J.Pan; J.Alloys Comp., **552**, 70-75 **(2013)**.
[42] V.Mote, Y.Purushotham, B.Dole; J.Theor.Appl. Phys., **6**, 6 **(2012)**.
[43] N.Saleema, M.Farzaneh; Appl.Surf.Sci., **254**, 2690-2695 **(2008)**.
[44] C.Wang, J.Xiao, J.Zeng, D.Jiang, Z.Yuan; Mater.Chem.Phys., **135**, 10-15 **(2012)**.
[45] C.Badre, T.Pauporté, M.Turmine, D.Lincot; Nanotechnol., **18**, 365705 **(2007)**.